Chemical Science

EDGE ARTICLE

View Article Online
View Journal | View Issue

Electrochemical formation and reactivity of a manganese peroxo complex: acid driven H_2O_2 generation *vs.* O–O bond cleavage†

Cite this: *Chem. Sci.*, 2014, **5**, 2304

H. Y. Vincent Ching,[ab] Elodie Anxolabéhère-Mallart,*[a] Hannah E. Colmer,[c] Cyrille Costentin,[a] Pierre Dorlet,[d] Timothy A. Jackson,[c] Clotilde Policar*[a] and Marc Robert[a]

Received 17th December 2013
Accepted 14th February 2014

DOI: 10.1039/c3sc53469c

www.rsc.org/chemicalscience

The formation of a side-on peroxo $[Mn^{III}L(O_2)]$ complex (L = phenolato-containing pentadentate ligand), resulting from the reaction of electrochemically reduced O_2 and $[Mn^{II}L]^+$, is monitored in DMF using cyclic voltammetry, low temperature electronic absorption spectroscopy and electron paramagnetic resonance spectroscopy. Mechanistic studies based on cyclic voltammetry reveal that upon addition of a strong acid the Mn–O bond is broken, resulting in the release of H_2O_2, whereas in the presence of a weak acid the O–O bond is cleaved *via* a concerted dissociative electron transfer. This dichotomy of M–O *versus* O–O bond cleavage is unprecedented for peroxomanganese(III) complexes and the latter offers a route for electrochemical O_2 activation by a manganese(II) complex.

Transition metal peroxo (M–OO) and hydro-peroxo (M–OOH) adducts are postulated as key intermediates in various catalytic oxygenation reactions, such as transition metal catalyzed oxidation of organic compounds,[1,2] as well as in fundamental enzymatic reactions, such as respiration[3,4] and photosynthesis.[5,6] In four-electron water oxidation and four-electron O_2 reduction, these intermediates are involved in a key step of the mechanism, *i.e.* the formation and the cleavage of the O–O bond, respectively.[7] Similar peroxo and hydro-peroxo intermediates have been shown to play a significant role in reactions involving the cleavage of the M–O bond, such as in the case of manganese superoxide dismutase (Mn-SOD), in the reduction step producing H_2O_2 from superoxide.[8–10] Proper control of the proton delivery to the peroxo intermediate is an important parameter that governs the gating of M–O *versus* O–O bond cleavage.[11] In the case of manganese, a number of biomimetic, mononuclear MnOO complexes have been reported resulting from a reaction with dioxygen,[12,13] potassium superoxide,[14–17] hydrogen peroxide[18–26] or superoxide produced by pulsed radiolysis.[27–30] A handful of peroxomanganese(III) complexes have been structurally characterized by X-ray crystallography and they all exhibit side-on (η^2) peroxo ligands.[14,18,23] Spectroscopic and density functional theory (DFT) computational studies support hexacoordination for $Mn^{III}OO$ adducts, with an ancillary ligand bound in a tetradentate manner.[20,21]

In spite of these recent reports of peroxomanganese(III) complexes, the present understanding of the reactivity of these complexes is not nearly as advanced as that of corresponding peroxo–iron[31] and peroxo–copper systems.[32] For example, reactivity studies of non-porphyrin peroxomanganese(III) complexes have focused predominantly on nucleophilic reactivity, such as the deformylation of aldehydes.[12,33,34] There are few reports on O–O activation affected by non-porphyrin peroxomanganese(III) species. Some of us have reported that a peroxomanganese(III) complex supported by an aminopyridyl ligand, $[Mn^{III}(O_2)(L5)]^+$ (L5 = *N*-methyl-*N*,*N*′,*N*′-tris(2-pyridylmethyl)ethane-1,2-diamine), reacts with acid to generate 2-pyridinecarboxylate, which is formed by oxidation of the L5 ligand.[19] This work thus offered a precedent for acid-assisted formation of a strong oxidant by a peroxomanganese(III) species, but the mechanism for the formation of the oxidant is unclear. More recently, Kovacs and coworkers have provided evidence that alkylperoxomanganese(III) complexes, featuring anionic N_4S ligands, decay by rate-limiting homolytic cleavage of the O–O bond.[35] Lastly, the group of Borovik reported a peroxomanganese(III) adduct to be an intermediate in the chemical reduction of O_2 to H_2O, using a mononuclear manganese complex that includes a hydrogen-

[a]*Univ Paris Diderot, Sorbonne Paris Cité, Laboratoire d'Electrochimie Moléculaire, UMR 7591 CNRS, 15 rue Jean-Antoine de Baïf, F-75205 Paris Cedex 13, France. E-mail: elodie.anxolabehere@univ-paris-diderot.fr; Fax: +33 157278788; Tel: +33 157278784*

[b]*Laboratoire des BioMolécules, CNRS UMR7203, Université Pierre et Marie Curie, Département de Chimie de l'ENS, 24, rue Lhomond, 75005 Paris, France. E-mail: clotilde.policar@ens.fr; Fax: +33 1 44 32 24 02; Tel: +33 1 44 32 24 20*

[c]*The University of Kansas, Chemistry Department, 1251 Wescoe Hall Drive, Lawrence, KS 66045, USA*

[d]*CNRS, Laboratoire Stress Oxydant et Détoxication, UMR 8221, Bât 532 CEA Saclay, 91191 Gif-sur-Yvette Cedex, France*

† Electronic supplementary information (ESI) available: Experimental details, additional data, CV analysis, parameters for CV simulations, and results and discussion for DFT computations. See DOI: 10.1039/c3sc53469c

bonding ligand.[13] A key step in this cycle is the reduction of the peroxomanganese(III) intermediate by diphenylhydrazine. However, no kinetic/mechanistic insights into this reaction were reported.

In the present work we (i) report the preparation and spectroscopic properties of a novel mononuclear peroxomanganese(III) adduct resulting from the reaction of electrochemically reduced O_2 and a Mn(II) complex, (ii) discuss the reactivity of the peroxo complex in various protic media by means of cyclic voltammetry (CV) and UV-vis absorption spectroscopy. The unprecedented electrochemical approach described herein allows for a mechanistic comparison of Mn–O and O–O bond cleavage reactions and for a new peroxomanganese(III) intermediate. The study reveals that in the presence of a strong acid, the Mn–O bond is broken, resulting in the release of H_2O_2, whereas in the presence of a weak acid, the O–O bond is cleaved *via* a concerted dissociative electron transfer. Importantly, the peroxo ligand in this system is derived from molecular oxygen. Thus, this work not only describes a new method for electrochemical O_2 activation by a manganese centre, but also provides insights into factors affecting the gating of M–O *versus* O–O bond cleavage by peroxometal species.

$[Mn^{III}L(O_2)]$ (LH = *N*-(2-hydroxybenzyl)-*N*,*N*′-bis[2-(*N*-methylimidazolyl)methyl]ethane-1,2-diamine) was prepared *in situ* from $[Mn^{II}L]^+$,[36] by exploiting the known electrochemical properties of O_2 in anhydrous *N*,*N*′-dimethylformamide (DMF).[37] At 293 K, CV of O_2 in anhydrous DMF exhibits a reversible, one-electron wave ($E^\circ = -0.865$ V *vs.* SCE) followed by a second irreversible, one-electron wave ($E^\circ \approx -2.5$ V *vs.* SCE), corresponding to the reductions $O_2/O_2^{\bullet-}$ and $O_2^{\bullet-}/H_2O_2$ (through a concerted proton and electron transfer (CPET) process with residual water as an acid),[38] respectively (Fig. S1†). The loss in reversibility of the $O_2/O_2^{\bullet-}$ wave upon addition of a Mn-complex can be used to test its reactivity towards a superoxide, as we and others have previously shown.[15,28,39] Upon addition of $[Mn^{II}L]^+$, the $O_2/O_2^{\bullet-}$ wave undergoes several changes. A pre-peak appears at a more positive potential value, together with the loss of reversibility of the $O_2/O_2^{\bullet-}$ wave (Fig. 1). These observations are in agreement with the formation of a $[Mn^{III}L(O_2)]$ adduct according to an EC mechanism (electron transfer + chemical reaction, Scheme 1). In the present experimental conditions, the pre-peak intensity is governed by both the concentration of $[Mn^{II}L]^+$ and its diffusion coefficient which is *ca.* ten times lower than that of O_2 (see ESI†). Consequently, when the $[Mn^{II}L]^+$ concentration at the electrode surface becomes nil, some O_2 remains to be reduced. Thus, even after adding the Mn complex in stoichiometric or slightly higher concentrations, the $O_2/O_2^{\bullet-}$ reduction wave ($E_p = -0.88$ V *vs.* SCE) can still be seen on the voltammograms. Complete reversibility loss occurs in the presence of 1.2 equivalents of the complex. Using parameters evaluated from the simulations of $O_2/O_2^{\bullet-}$ reduction and $[Mn^{II}L]^+/[Mn^{III}L]^{2+}$ oxidation waves (Fig. S1 and 2, Table S1†), the irreversible wave shown in Fig. 1 could be modelled as a simple EC mechanism, with a fast, irreversible chemical reaction ($k = 10^{10}$ M^{-1} s^{-1}) (reactions 1 and 1a).[40] The peroxomanganese(III) adduct is relatively stable on the experimental cyclic voltammetry timescale and can be re-oxidized. Indeed, as shown in Fig. 2, after scanning towards negative potentials and generating the $[Mn^{III}L(O_2)]$ adduct at the electrode surface, the oxidation of this species is detected on the reverse scan towards positive potentials (see ESI† for the simulation of this wave).

$[Mn^{III}L(O_2)]$ was also characterized by UV-vis spectro-electrochemistry using the same method as the one recently reported for closely related Mn(II) complexes.[41] During controlled potential electrolysis performed at −1.2 V *vs.* SCE ($T = 263$ K), a colourless solution containing O_2 and $[Mn^{II}L]^+$ (1 : 1) turned yellow with a new absorption band at $\lambda = 440$ nm ($\varepsilon = 600$ M^{-1} cm^{-1}) and a shoulder at 540 nm ($\varepsilon = 226$ M^{-1} cm^{-1}) (Fig. 2, right panel). The λ and ε values of the latter band are similar to those reported for a six-coordinate (η_2)-peroxomanganese(III) species prepared from related Mn(II) complexes and a superoxide[17,20,21] or hydrogen peroxide.[19–21] Aliquots of the electrolyzed solution were collected for EPR analysis and frozen at once. The X-band parallel-mode EPR spectra, recorded at 4 K, showed a six-line signal with a 5 mT separation and centered at 77 mT ($g = 8.7$) (Fig. S6†), characteristic of a monomeric Mn(III) complex ($S = 2$).[12,17,42]

Finally, DFT computational studies[43] on $[Mn^{III}L(O_2)]$ led to the identification of stable monomeric structures with

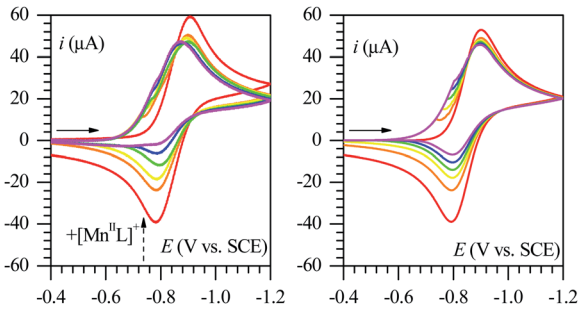

Fig. 1 Left panel: CV spectra of O_2 (1.0 mM, air saturated) in DMF + 0.1 M Bu_4NPF_6 with an increasing concentration of $[Mn^{II}L]^+$: 0 (red), 0.4 (orange), 0.6 (yellow), 0.8 (green), 1.0 (blue), and 1.2 (magenta) mM at 0.2 V s^{-1} at a glassy carbon disk electrode ($T = 293$ K). Right panel: simulations. See ESI† for the details of the simulation parameters.

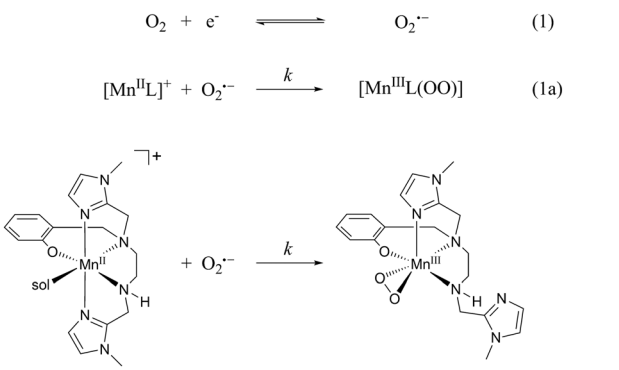

Scheme 1 $[Mn^{II}L]^+$ and $[Mn^{III}L(O_2)]$ peroxo adduct (see text) in a DMF solution (sol = DMF).

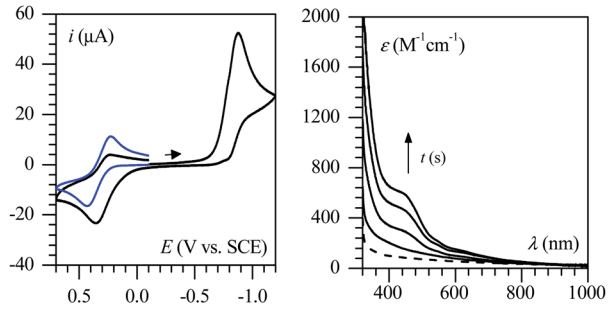

Fig. 2 Left panel: CV spectra of $[Mn^{II}L]^+$ (1.2 mM) and O_2 (1.0 mM, air saturated) in DMF + 0.1 M Bu_4NPF_6 at 0.2 V s^{-1} at a glassy carbon disk electrode (T = 293 K), scanning towards cathodic (black trace) and anodic (blue trace) potentials. Right panel: evolution of UV-vis spectra upon electrolysis performed at −1.2 V *vs.* SCE at 263 K (200 s, 1 spectrum per 50 s), the experimental conditions were identical to the ones used for CV in the left panel.

hexacoordinate Mn^{III} centres, with a side-on peroxo ligand and a tetradentate L ligand (Fig. S7†). For two of the models, the tetradentate binding mode of the L ligand is achieved through dissociation of a methylimidazolyl moiety, while the phenolato ligand is *cis* with respect to the peroxo as illustrated in Scheme 1. A structure with a peroxo ligand bound in an end-on fashion – in which case the phenolato is *trans* to the peroxo unit – is at a much higher total energy (~16 kcal mol^{-1}) and thus appears unlikely. These results remain true regardless of whether the energy calculations are performed in the gas phase or are incorporating solvation effects from DMF using the COSMO method (Table S3†).[44] TD-DFT-computed electronic absorption spectra[45] for models with a side-on peroxo ligand are in good agreement with the experimental spectrum of the $[Mn^{III}L(O_2)]$ species, further confirming its monomeric nature as well as the oxygen binding mode (Fig. S8†).

Addition of perchloric acid. Towards H_2O_2 formation

Upon addition of increasing amounts of $HClO_4$ from 3 to 6 mM (completely dissociated in DMF),[46] the voltammogram of an oxygenated solution of $[Mn^{II}L]^+$ (10 mM)[47] shows two remarkable features (Fig. 3): (i) the intensity of the previously observed irreversible cathodic wave increases from one electron to two electrons; (ii) a crossing between the forward and backward traces is observed, indicative of a reduction process on the reverse scan. Additionally, the intensity of the $[Mn^{II}L]^+/[Mn^{III}L]^{2+}$ oxidation wave decreases proportionally to the amount of $HClO_4$ added (Fig. S9†), which is in line with a fast and irreversible protonation of the ligand L, presumably a protonation of the phenolato moiety, leading to decomposition of the complex and formation of both protonated ligand LH and Mn^{2+} ion in solution. This was confirmed by UV-vis experiments (see Fig. S10†). Consequently, upon running cyclic voltammetry experiments in the presence of O_2, $[Mn^{II}L]^+$ in excess, and added $HClO_4$, the acid actually present in solution is LH. The various steps taking place at the level of the O_2 reduction wave are summarized in

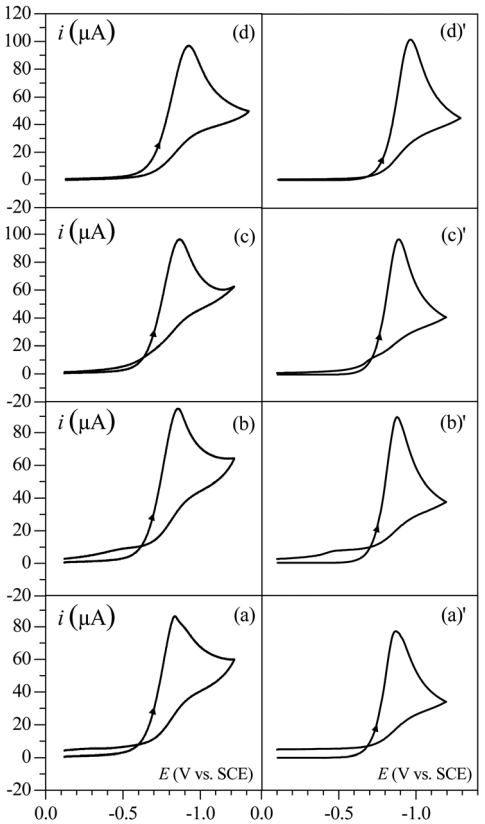

Fig. 3 CV spectra of $[Mn^{II}L]^+$ (10 mM) and O_2 (1.0 mM, air saturated) with increasing $[HClO_4]$ in DMF + 0.1 M Bu_4NPF_6 at 0.2 V s^{-1} at a glassy carbon disk electrode (T = 293 K): from bottom to top: 3 (a, a′), 4 (b, b′), 5 (c, c′), 6 (d, d′) mM. Left panel: experimental waves (a–d); right panel: simulations according to the mechanism depicted in Scheme 2(a′)–(d′). See ESI† for details of the simulation parameters.

Scheme 2. Once formed at the electrode surface, the superoxide anion can be protonated by LH, forming $HO_2^{\bullet}$ which is reduced to HO_2^- at the electrode surface according to an ECE mechanism or in solution involving a DISP mechanism,[48] thus leading to a two-electron wave (reactions (2)–(4), Scheme 2). However, the superoxide ion competitively reacts with $[Mn^{II}L]^+$ to form $[Mn^{III}L(O_2)]$. In the presence of LH, $[Mn^{III}L(O_2)]$ is protonated and the Mn–O bond is cleaved, leading to the decoordination of HO_2^- and $[Mn^{III}L]^{2+}$ (reaction (3′), Scheme 2). A second electron transfer occurs at the electrode surface because $[Mn^{III}L]^{2+}$ is formed at a potential much more negative than the $[Mn^{III}L]^{2+}/[Mn^{II}L]^+$ standard potential (reactions (4′) and (5′), Scheme 2). The classical two-electron ECE/DISP mechanism for O_2 reduction in the presence of an acid (in this case LH) is thus in competition with another two-electron ECE process (referred to as ECE', Scheme 2) with a minor DISP' counterpart. The DISP' counterpart corresponds to the reduction of $[Mn^{III}L]^{2+}$ in solution by a superoxide ion, whose concentration remains very small in the diffusion layer due to its fast reaction with excess $[Mn^{II}L]^+$. The experimental observation of a crossing between the forward and backward CV traces is thus attributed to the fact that the ECE' pathway overcomes the classical ECE/DISP process with the formation of $[Mn^{III}L]^{2+}$ in solution, followed by its diffusion

ECE/DISP

$$O_2 + e^- \rightleftharpoons O_2^{\bullet -} \quad (1)$$

$$LH + O_2^{\bullet -} \xrightarrow{k_H} HOO^{\bullet} + L^- \quad (2)$$

$$HOO^{\bullet} + e^- \rightleftharpoons HOO^- \quad (3)$$

$$HOO^{\bullet} + O_2^{\bullet -} \xrightarrow{k_{disp}} HOO^- + O_2 \quad (4)$$

$$HOO^- + LH \xrightarrow{k_H} H_2O_2 + L^- \quad (5)$$

ECE'/DISP'

$$O_2 + e^- \rightleftharpoons O_2^{\bullet -} \quad (1)$$

$$[Mn^{II}L]^+ + O_2^{\bullet -} \xrightarrow{k_{df}} [Mn^{III}L(OO)] \quad (2')$$

$$[Mn^{III}L(OO)] + LH \xrightarrow{k_p} [Mn^{III}L]^{2+} + HOO^- + L^- \quad (3')$$

$$[Mn^{III}L]^{2+} + e^- \rightleftharpoons [Mn^{II}L]^+ \quad (4')$$

$$[Mn^{III}L]^{2+} + O_2^{\bullet -} \xrightarrow{k'_{disp}} [Mn^{II}L]^+ + O_2 \quad (5')$$

$$HOO^- + LH \xrightarrow{k_H} H_2O_2 + L^- \quad (5)$$

Scheme 2 Oxygen reduction mechanism leading to H_2O_2 in the presence of a strong acid and $[Mn^{II}L]^+$.

towards the electrode. $[Mn^{III}L]^{2+}$ is then reduced at the electrode, thus generating a reduction current in the reverse scan (reaction (4′), Scheme 2).

As seen in Fig. 3, an excellent match between the simulated and experimental voltammograms is obtained, thus validating the proposed mechanism (see ESI† for details of the simulation). It is also remarkable that the trace crossing is well reproduced at all acid concentrations. It further allows for an estimate of the apparent protonation Mn–O bond cleavage rate constant $k_p = 10^5$ M^{-1} s^{-1}. At a large $HClO_4$ concentration, the crossing between the forward and the reverse scan (at *ca.* −0.7 V *vs.* SCE) tends to vanish because of a weaker reduction current due to the fact that the $[Mn^{II}L]^+$ concentration decreases concomitantly to ligand protonation and decoordination (LH formation). Hence, the ECE/DISP pathway prevails over the ECE' mechanism (reaction (2) overcomes reaction (2′), Scheme 2). The cleavage of the Mn–O bond was also proven by UV-vis experiments. Indeed, upon addition of one equivalent of $HClO_4$, the spectra of the $[Mn^{III}L(O_2)]$ solution (prepared by electrolysis as shown in Fig. 2, right panel) show the formation of the $[Mn^{III}L]^{2+}$ complex (Fig. S11†).

Addition of a weak acid. Towards O–O bond cleavage

In the presence of a weak acid (*e.g.* H_2O, pK_a = 31.5 in DMF),[49] electrochemically generated $[Mn^{III}L(O_2)]$ is stable since the intensity of the irreversible O_2 reduction wave does not increase to a two-electron transfer (*i.e.* the protonation of the peroxo species, leading to the release of H_2O_2 and coupled with $[Mn^{III}L]^{2+}/[Mn^{II}L]^+$ reduction, no longer occurs, Fig. S12†). However, $[Mn^{III}L(O_2)]$ was reduced at a more negative potential (∼−1.65 V *vs.* SCE, Fig. 4, top left panel). A closely similar reduction wave is also observed when $[Mn^{III}L(O_2)]$ was chemically prepared *in situ* by the addition of [K(18-crown-6)]O_2 to $[Mn^{II}L]^+$ at a low temperature (Fig. S5b†). Note also that this reduction wave peaking at −1.65 V could not be due to H_2O_2 since it is reduced beyond −2.7 V *vs.* SCE at the carbon electrode. Therefore, the wave at −1.65 V must be due to the reduction of the $[Mn^{III}L(O_2)]$ complex.

From the height and shape of the $[Mn^{III}L(O_2)]$ reduction wave, and after considering the diffusion coefficient value of the Mn complexes, it is concluded that the reaction involves a two-electron transfer process. We thus propose that the addition of two electrons to the peroxomanganese(III) complex leads to the cleavage of the O–O bond because neither the manganese centre, nor the ligand, can sustain the electron density. The resultant dioxomanganese(III) intermediate ($[Mn^{III}L(O_2)]^{2-}$) is readily protonated by residual or added H_2O to give a dihydroxomanganese(III) complex $[Mn^{III}L(OH)_2]$, (Scheme 3). At time scales longer than those of cyclic voltammetry, the $[Mn^{III}L(OH)_2]$ complex is likely to evolve, potentially to multinuclear Mn species, especially considering that terminal hydroxomanganese(III) complexes are generally unstable unless sterically protected.[50] Not surprisingly, attempts to characterize the putative $[Mn^{III}L(OH)_2]$ species have been hampered by its instability. Nonetheless, UV-vis spectra collected during electrolysis at −1.9 V show that the signal associated with $[Mn^{III}L(O_2)]$ evolves to give a

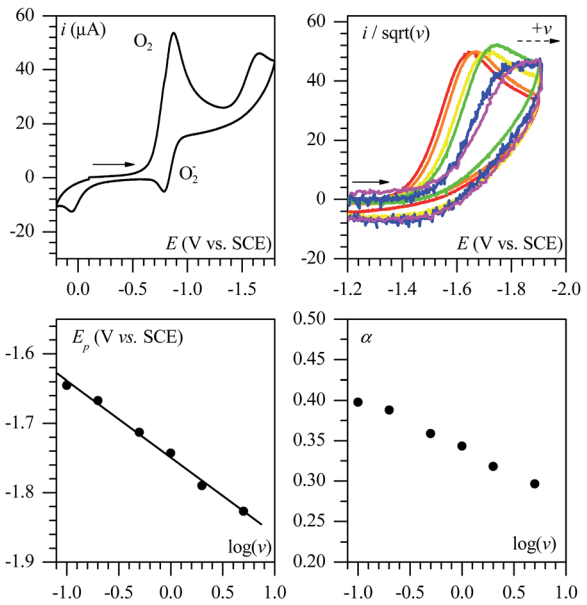

Fig. 4 CV spectra of O_2 (1.0 mM, saturated air) in DMF + 0.1 M Bu_4NPF_6 at a glassy carbon disk electrode (T = 293 K). Top left panel: with $[Mn^{II}L]^+$ (1.2 mM) at 0.2 V s^{-1}. Top right panel: normalized CV with $[Mn^{II}L]^+$ (2 mM) after a 10 s pre-electrolysis (E = −1.2 V *vs.* SCE) at varying scan rates (v): 0.1 (red), 0.2 (orange), 0.5 (yellow), 1 (green), 2 (blue), and 5 (magenta) V s^{-1}. Bottom left panel: peak potential of the two-electron wave as a function of log(v). Bottom right panel: transfer coefficient values (α) as a function of log(v), as determined from the peak width values.

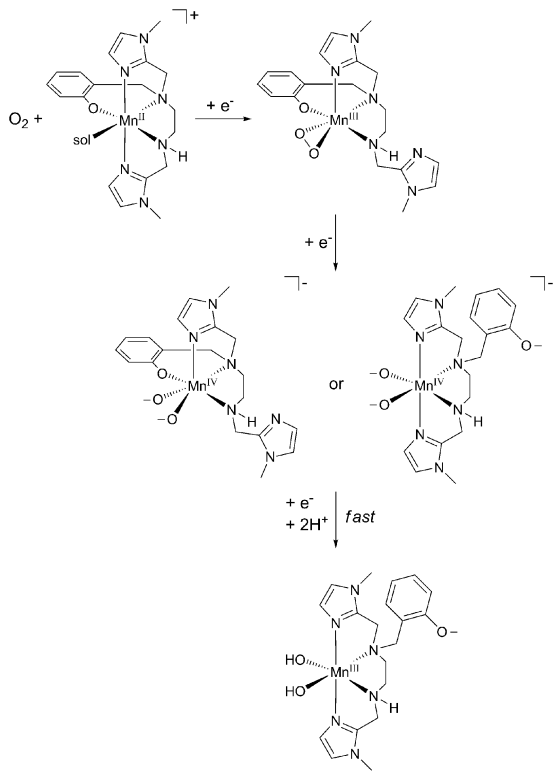

Scheme 3 Proposed mechanism for electrochemical preparation and reduction of $[Mn^{III}L(O_2)]$ in weakly protic media.

broad signal of moderate intensity that tails after 600 nm (Fig. S15†). This end spectrum is consistent with oxidized Mn^{III} (or Mn^{IV}) species, and not Mn^{II}. Thus, the UV-vis data collected during electrolysis provide corroborating evidence that the two-electron reduction is ligand, and not metal, centred.[51]

This two-electron wave remains unaffected even in the presence of a large acid concentration (*e.g.* H_2O ~ 500 equivalents, Fig. S13†), suggesting that protonation is not the rate determining step of the process. Further analysis of the wave in the presence of two equivalents of $[Mn^{II}L]^+$ and after a 10 s pre-electrolysis at −1.2 V *vs.* SCE (in order to generate a constant concentration of $[Mn^{III}L(O_2)]$ species at the electrode surface) shows that the variation of the peak potential (E_p) with respect to the scan rate is $\partial E_p/\partial \log v = -110$ mV per decade, along with a large peak-width (Fig. 4, upper right panel and bottom left panel). This leads to the unambiguous conclusion that the two-electron $[Mn^{III}L(O_2)]$ reduction wave is kinetically controlled by the initial electron transfer with a small transfer coefficient ($\alpha = 1.856(RT/F)/(E_{p/2} - E_p)$) close to 0.35 (Fig. 4, bottom right panel).[48] Such a small α value is indicative of a large reorganization energy according to the Marcus theory for electron transfer. More precisely, the free energy of activation ($\Delta G^{\neq}_{peak}$) can be estimated at the peak of the voltammetric wave and the total reorganization energy λ then ensues (see ESI†):[48]

$$\Delta G^{\neq}_{peak} = 0.36 \text{ eV} \text{ and } \lambda = \frac{\Delta G^{\neq}_{peak}}{\alpha^2} \approx 2.93 \text{ eV}$$

This large total reorganization energy is perfectly compatible with an initial electron transfer concerting the O–O bond breaking process,[52] a pathway that bypasses the high energy $[Mn^{II}L(O_2)]^-$ intermediate. In that case, λ comprises the cumulative contributions from the homolytic O–O bond dissociation energy, the solvent reorganization energy as well as the internal reorganization energy due to structural changes from the oxidized to the reduced state. This latter contribution may possibly involve the decoordination of the phenolato moiety. Indeed, on the reverse scan after the two-electron reduction, a new irreversible oxidation wave is observed at *ca.* 0 V (Fig. 4, top left panel). It was assigned to the oxidation of the phenolato anion by comparison with the cyclic voltammetry of L. Finally, additional internal reorganization energy may also involve a ligand rearrangement due to the pendant imidazolyl moiety present in $[Mn^{III}L(O_2)]$ that can readily coordinate to the metal centre, filling the vacancy left by the departing phenolato moiety. The above discussion leads to the mechanism depicted in Scheme 3 for the electrochemical O_2 reduction in the presence of $[Mn^{II}L]^+$ in weakly protic media.

It is worth noting that DFT calculations indicate that the one-electron reduced $[Mn^{II}L(O_2)]^-$ form is much higher in energy than the $[Mn^{IV}L(O)_2]^-$ form (see ESI†), with a standard potential close to −2.0 V *vs.* SCE. Such a negative standard potential is not compatible with a stepwise process in which a fast O–O bond cleavage would follow an initial, slow electron transfer occurring at $E_p \approx -1.65$ V *vs.* SCE, thus giving a further confirmation that the process is indeed a concerted O–O bond breaking-electron transfer. It is seen in Scheme 3 that O_2 is formally electrochemically reduced to H_2O (OH^-) in DMF in the presence of $[Mn^{II}L]^+$ at the second reduction wave. In the same potential range, O_2 without the metal complex is reduced to H_2O_2 (Fig. S14†).

In conclusion, the electrochemical formation and reactivity of a novel peroxomanganese(III) complex with a phenolato-containing pentadentate ligand has been described. The oxidative addition of electrochemically generated $O_2^{\bullet -}$ to $[Mn^{II}L]^+$ yielded $[Mn^{III}L(O_2)]$, a peroxo complex in which the oxygen–oxygen bond is weakened. Mechanistic studies based on cyclic voltammetry reveal that upon addition of a strong acid ($HClO_4$), the Mn–O bond is broken resulting in the release of H_2O_2. In the presence of a weak acid (H_2O), $[Mn^{III}L(O_2)]$ is reduced through a two-electron process. The formation of the putative $[Mn^{III}L(OH)_2]$ is proposed to occur according to $[Mn^{III}L(O_2)] + 2e^- + 2H^+ \rightarrow [Mn^{III}L(OH)_2]$. This reductive process is kinetically controlled by the first electron transfer, concerting the O–O bond cleavage. This pathway bypasses the high $[Mn^{II}L(O_2)]^-$ intermediate. To the best of our knowledge, this electrochemical approach is the first example of a mechanistic study of acid driven H_2O_2 formation *vs.* concerted reductive O–O bond cleavage in a peroxo–metal complex, and it has delivered new insights into O_2 activation reactivity by such species.

Acknowledgements

Partial financial support from the Agence Nationale de la Recherche (ANR 2010 BLAN 0808) and French Infrastructure for

Integrated Structural Biology (FRISBI) ANR-10-INSB-05-01 is gratefully acknowledged. H.Y.V.C. was supported by ANR 2010 BLAN 0808. T.A.J. acknowledges financial support from the US NSF (CHE-1056470). H.E.C. was supported by NIH-GMS T32 GM08545.

Notes and references

1 W. Nam, *Acc. Chem. Res.*, 2007, **40**, 465–634.
2 B. Meunier, in *Biomimetic Oxidations Catalyzed by Transition Metal Complexes*, ed. B. Meunier, Imperial College Press, London, 2000.
3 S. Ferguson-Miller and G. T. Babcock, *Chem. Rev.*, 1996, **96**, 2889–2907.
4 W. B. Tolman and E. I. Solomon, *Inorg. Chem.*, 2010, **49**, 3555–3556.
5 C. Tommos and G. T. Babcock, *Acc. Chem. Res.*, 1998, **31**, 18–25.
6 J. Messinger, *Phys. Chem. Chem. Phys.*, 2004, **6**, 4764–4771.
7 C. J. Chang, M. C. Chang, N. H. Damrauer and D. G. Nocera, *Biochim. Biophys. Acta*, 2004, **1655**, 13–28.
8 C. Bull, E. C. Niederhoffer, T. Yoshida and J. A. Fee, *J. Am. Chem. Soc.*, 1991, **113**, 4069–4076.
9 A. S. Hearn, C. K. Tu, H. S. Nick and D. N. Silverman, *J. Biol. Chem.*, 1999, **274**, 24457–24460.
10 T. A. Jackson, A. Karapetian, A.-F. Miller and T. C. Brunold, *Biochemistry*, 2005, **44**, 1504–1520.
11 J. Rosenthal and D. G. Nocera, *Acc. Chem. Res.*, 2007, **40**, 543–553.
12 R. L. Shook, W. A. Gunderson, J. Greaves, J. W. Ziller, M. P. Hendrich and A. S. Borovik, *J. Am. Chem. Soc.*, 2008, **130**, 8888–8889.
13 R. L. Shook, S. M. Peterson, J. Greaves, C. Moore, A. L. Rheingold and A. S. Borovik, *J. Am. Chem. Soc.*, 2011, **133**, 5810–5817.
14 R. B. VanAtta, C. E. Strouse, L. K. Hanson and A. M. Valentine, *J. Am. Chem. Soc.*, 1987, **109**, 1425–1434.
15 C. Policar, S. Durot, F. Lambert, M. Cesario, F. Ramiandrasoa and I. Morgenstern-Badarau, *Eur. J. Inorg. Chem.*, 2001, 1807–1818.
16 S. Durot, C. Policar, F. Cisnetti, F. Lambert, J.-P. Renault, G. Pelosi, G. Blain, H. Korri-Youssifi and J.-P. Mahy, *Eur. J. Inorg. Chem.*, 2005, **14**, 3513–3523.
17 S. Groni, G. Blain, R. Guillot, C. Policar and E. Anxolabéhère-Mallart, *Inorg. Chem.*, 2007, **46**, 1951–1953.
18 N. Kitajima, H. Komatsuzaki, S. Hikichi, M. Osawa and Y. Moro-Oka, *J. Am. Chem. Soc.*, 1994, **116**, 11596–11597.
19 S. Groni, P. Dorlet, G. Blain, S. Bourcier, R. Guillot and E. Anxolabéhère-Mallart, *Inorg. Chem.*, 2008, **47**, 3166–3172.
20 R. A. Geiger, S. Chattopadhyay, V. W. Day and T. A. Jackson, *J. Am. Chem. Soc.*, 2010, **132**, 2821–2831.
21 R. A. Geiger, D. F. Leto, S. Chattopadhyay, P. Dorlet, E. Anxolabéhère-Mallart and T. A. Jackson, *Inorg. Chem.*, 2011, **50**, 10190–10203.
22 U. P. Singh, A. K. Sharma, S. Hikichi, H. Komatsuzaki, Y. Moro-oka and M. Akita, *Inorg. Chim. Acta*, 2006, **359**, 4407–4411.
23 M. S. Seo, J. Y. Kim, J. Annaraj, Y. Kim, Y.-M. Lee, S.-J. Kim, J. Kim and W. Nam, *Angew. Chem., Int. Ed.*, 2007, **46**, 377–380.
24 J. Annaraj, J. Cho, Y.-M. Lee, S. Y. Kim, R. Latifi, S. P. de Visser and W. Nam, *Angew. Chem., Int. Ed.*, 2009, **48**, 4150–4153.
25 R. A. Geiger, G. B. Wijeratne, V. W. Day and T. A. Jackson, *Eur. J. Inorg. Chem.*, 2012, 1598–1608.
26 R. A. Geiger, S. Chattopadhyay, V. W. Day and T. A. Jackson, *Dalton Trans.*, 2011, **40**, 1707–1715.
27 D. E. Cabelli and B. H. J. Bielski, *J. Phys. Chem.*, 1984, **88**, 3111–3115.
28 Y. Nishida, N. Tanaka, A. Yamazaki, T. Tokii, N. Hashimoto, K. Ide and K. Iwasawa, *Inorg. Chem.*, 1995, **34**, 3616–3620.
29 S. Durot, F. Lambert, J.-P. Renault and C. Policar, *Eur. J. Inorg. Chem.*, 2005, 2789–2793.
30 K. Barnese, E. B. Gralla, D. E. Cabelli and J. S. Valentine, *J. Am. Chem. Soc.*, 2008, **130**, 4604–4606.
31 M. Costas, M. P. Mehn, M. P. Jensen and L. Que Jr, *Chem. Rev.*, 2004, **104**, 939.
32 C. J. Cramer and W. B. Tolman, *Acc. Chem. Res.*, 2007, **40**, 601.
33 J. Cho, R. Sarangi and W. Nam, *Acc. Chem. Res.*, 2012, **45**, 1321–1330.
34 R. A. Geiger, S. Chattopadhyay, V. W. Day and T. A. Jackson, *Dalton Trans.*, 2011, **40**, 1707–1715.
35 M. K. Coggins, V. Martin-Diaconescu, S. DeBeer and J. A. Kovacs, *J. Am. Chem. Soc.*, 2013, **135**, 4260–4272.
36 F. Cisnetti, A.-S. Lefèvre, R. Guillot, F. Lambert, G. Blain, E. Anxolabéhère-Mallart and C. Policar, *Eur. J. Inorg. Chem.*, 2007, 4472–4480.
37 D. T. Sawyer and J. S. Valentine, *Acc. Chem. Res.*, 1981, **14**, 393–400.
38 C. Costentin, D. H. Evans, M. Robert, J.-M. Savéant and P. S. Singh, *J. Am. Chem. Soc.*, 2005, **127**, 12490–12491.
39 A. Deroche, I. Morgenstern-Badarau, M. Cesario, J. Guilhem, B. Keita, L. Nadjo and C. Houée-Levin, *J. Am. Chem. Soc.*, 1996, **118**, 4567–4573.
40 Due to the slow electron transfer kinetics of O_2 reduction, the chemical reaction rate constant cannot be measured. Changing the k value has no effect on the position of the pre-wave, which is indeed determined by the electron rate constant. Thus, the value of k is taken as diffusion limited.
41 S. El Ghachtouli, H. Y. V. Ching, B. Lassalle-Kaiser, R. Guillot, D. F. Leto, S. Chattopadhyay, T. A. Jackson, P. Dorlet and E. Anxolabéhère-Mallart, *Chem. Commun.*, 2013, **49**, 5696–5698.
42 K. A. Campbell, M. R. Lashley, J. K. Wyatt, M. H. Nantz and R. D. Britt, *J. Am. Chem. Soc.*, 2001, **123**, 5710–5719.
43 All calculations employed ORCA 2.91 and F. Neese, *WIREs Comput. Mol. Sci.*, 2012, **2**, 73.
44 S. Sinnecker, A. Rajendran, A. Klamt, M. Diedenhofen and F. Neese, *J. Phys. Chem. A*, 2006, **110**, 2235.
45 T. Petrenko, S. Kossmann and F. Neese, *J. Chem. Phys.*, 2011, **134**, 054116–054130.

46 *Acid-Base Dissociation Constants in Dipolar Aprotic Solvents, IUPAC Chemical Data Series, N° 35*, K. Izutsu, Blackwell Scientific Publications, Brookline Village, 1990, p. 166.
47 In order to favor the formation of $[Mn^{III}L(O_2)]$ over the $HO_2^{\bullet}$ radical formation (issued from the efficient protonation of the superoxide anion), the initial concentration of the Mn complex was in excess towards the proton concentration.
48 J.-M. Savéant, in *Elements of Molecular and Biomolecular Electrochemistry*, Wiley-Interscience, New-York, 2006.
49 C. P. Andrieux, J. Gamby, P. Hapiot and J.-M. Savéant, *J. Am. Chem. Soc.*, 2003, **125**, 10119–10124.
50 R. L. Shook and A. S. Borovik, *Inorg. Chem.*, 2010, **49**, 3646–3660.
51 Due to the instability of the samples, all attempts to detect the dihydroxomanganese(III) complex using ESI-MS were thwarted.
52 C. Costentin, M. Robert and J.-M. Savéant, *Chem. Phys.*, 2006, **324**, 40–56.